Journal of
Applied Remote Sensing

# Synthetic advanced baseline imager true-color imagery

Donald Hillger
Louie Grasso
Steven Miller
Renate Brummer
Robert DeMaria

# Synthetic advanced baseline imager true-color imagery

**Donald Hillger,[a] Louie Grasso,[b] Steven Miller,[b] Renate Brummer,[b] and Robert DeMaria[b]**

[a] Colorado State University, National Oceanic and Atmospheric Administration/National Environmental Satellite, Data, and Information Service/Center for Satellite Applications and Research/Regional and Mesoscale Meteorology Branch, CIRA – 1375, Fort Collins Colorado 80523-1375
Don.Hillger@NOAA.gov

[b] Colorado State University, Cooperative Institute for Research in the Atmosphere (CIRA), CIRA – 1375, Fort Collins Colorado 80523-1375

**Abstract.** True-color imagery, which is formed via a weighted combination of red, green, and blue (RGB) spectral information, has important operational applications for qualitative environmental characterization, including the detection of smoke plumes, volcanic ash, and other aerosols that are not as easily discerned in conventional visible or infrared imagery, but may be more readily characterized via color properties. Despite its universal popularity, true-color is currently unavailable from geostationary satellites, and the next-generation GOES-R advanced baseline imager (ABI) will fall one band (green; 0.55 $\mu$m) short of doing so. However, approximations exist, and a process for simulating true-color imagery representative of capabilities anticipated from the ABI is presented and assessed here. High-resolution atmospheric model simulations are used to produce the ABI reflective band imagery required for true-color imagery. Those simulations are then rendered at ABI spatial (0.5-km visible) and temporal (5 min) resolution, to provide realistic data, long before the anticipated 2015 launch of GOES-R. An additional analysis, a color-space transformation, is used to assess the true-color (RGB) ABI images. The resulting hue images verify the less-green bias in the synthetic-green band and synthetic-RGB images created on ABI simulated data. Assessing the deficiencies in the RGB process will hopefully lead to an improved and standard means for generating an RGB product from the ABI data stream. Finally, as one of the many product applications of true-color imagery, an example of synthetic true-color imagery with added smoke is presented. The incorporation of aerosol properties into simulated imagery may help reveal the limits of detectability for atmospheric aerosols with future ABI.  [DOI: 10.1117/1.3576112]

**Keywords:** GOES-R; advanced baseline imager; true-color; RGB; synthetic-green; simulated imagery.

Paper 10119R received Aug. 12, 2010; revised manuscript received Mar. 1, 2011; accepted for publication Mar. 18, 2011; published online Apr. 26, 2011.

## 1 Introduction

There are many applications for true-color and RGB imagery. Examples in published literature and on the Web include the detection and retrieval of smoke plumes, volcanic ash, and other aerosols.[1,2] Of the meteorological satellites in orbit, the true-color capability on the moderate resolution imaging spectroradiometer (MODIS) instrument provides the primary source of true-color capabilities. See the MODIS Web (http://modis.gsfc.nasa.gov/) for almost daily examples of either true-color imagery, or false-color imagery with eye-pleasing colors. Likewise, the NESDIS home page (http://www.nesdis.noaa.gov/) features color imagery

1931-3195/2011/$25.00 © 2011 SPIE

products derived from various National Oceanic and Atmospheric Administration (NOAA) polar-orbiting satellites currently in orbit, none of which currently have instruments with true-color capability.

True-color imagery is in fact a special case of a broader class of red-green-blue composite imagery, wherein spectral information is loaded into three color planes which are then combined to produce the full spectrum of possible colors. In the case of true-color, the information is loaded in a way that approximates the sensitivity and response of the cone cells of the human eye's retina for normal vision, such that the resultant imagery appears "true" to what the eye might observe (i.e., akin to a color photograph).

The Geostationary Operational Environmental Satellite (GOES)-R program office home page (http://www.goes-r.gov/) features a true-color image, reproduced in Fig. 1, where the static color background was obtained from MODIS imagery.[3] The example makes a tacit suggestion that true-color capability will be available directly from the advanced baseline imager (ABI).[4] Similarly, current GOES imagery at http://goes.gsfc.nasa.gov/ makes it look like GOES already has true-color capability, but that is done by adding the cloud features from current GOES imagery to a static background image with colored land features.

Current GOES contains only one of the three bands needed for true-color. Future GOES-R ABI will be an improvement, but it will contain only two of the three necessary bands required for true-color: a red (0.64 $\mu$m) band, and a blue (0.47 $\mu$m) band. The missing green (0.55 $\mu$m) band must be synthesized from the other available ABI bands in order to produce an RGB product.* A companion paper by Miller et al.[5] addresses the decision to not provide true-color capabilities with ABI on GOES-R

Another popular source of color imagery is shown in Fig. 2, from the *NexSat*[1] webpage (www.nrlmry.navy.mil/NEXSAT.html). *NexSat* previews selected capabilities of the next-generation polar-orbiting joint polar satellite system (JPSS†) series, with an emphasis on the visible/infrared imager/radiometer suite (VIIRS) sensor. These demonstrations extend to polar-orbiting/geostationary synergy applications. A particularly popular VIIRS/ABI synergy product found on *NexSat* is 'GeoColor' imagery shown in Fig. 2, which combines current geostationary cloud imagery with a static true-color background derived from MODIS blue marble data. The demonstration is intended to simulate the capability of a GOES-R ABI true-color product under the assumption of a synthesized Green band, supplied by a VIIRS-trained correlative technique (described by Miller et al.[5]).

Color is also heavily used by the television media for the display of satellite imagery aimed at the public, realizing that black and white imagery is passé to a computer and Web-literate populace. Several examples are found in the popular TV websites in the Denver-area market alone:

- Channel 4: http://weather.cbs4denver.com/US/CO/Denver/KDEN.html
- Channel 7: http://www.thedenverchannel.com/radarviews/index.html
- Channel 9: http://www.9news.com/weather/radar/national/

Besides satellite imagery, most other weather data provided by these outlets is also displayed in color. Color adds greatly to the ability to distinguish image features compared to gray shades, both for the layman as well as professional forecasters. True-color imagery in particular provides colors that would be expected if a viewer were observing the earth and its weather from space.

In line with the overwhelming use of color in so many venues, the ability to provide GOES-R images in true-color is both expected and possible. Here, a process for previewing the variety of

*In this paper, the term "synthetic" is reserved for the green and resulting RGB images, whereas the term "simulated" is reserved for the model-generated ABI to be introduced later.

†JPSS is the civilian series resulting from a reconfiguration of the national polar-orbiting operational environmental satellite system (NPOESS).

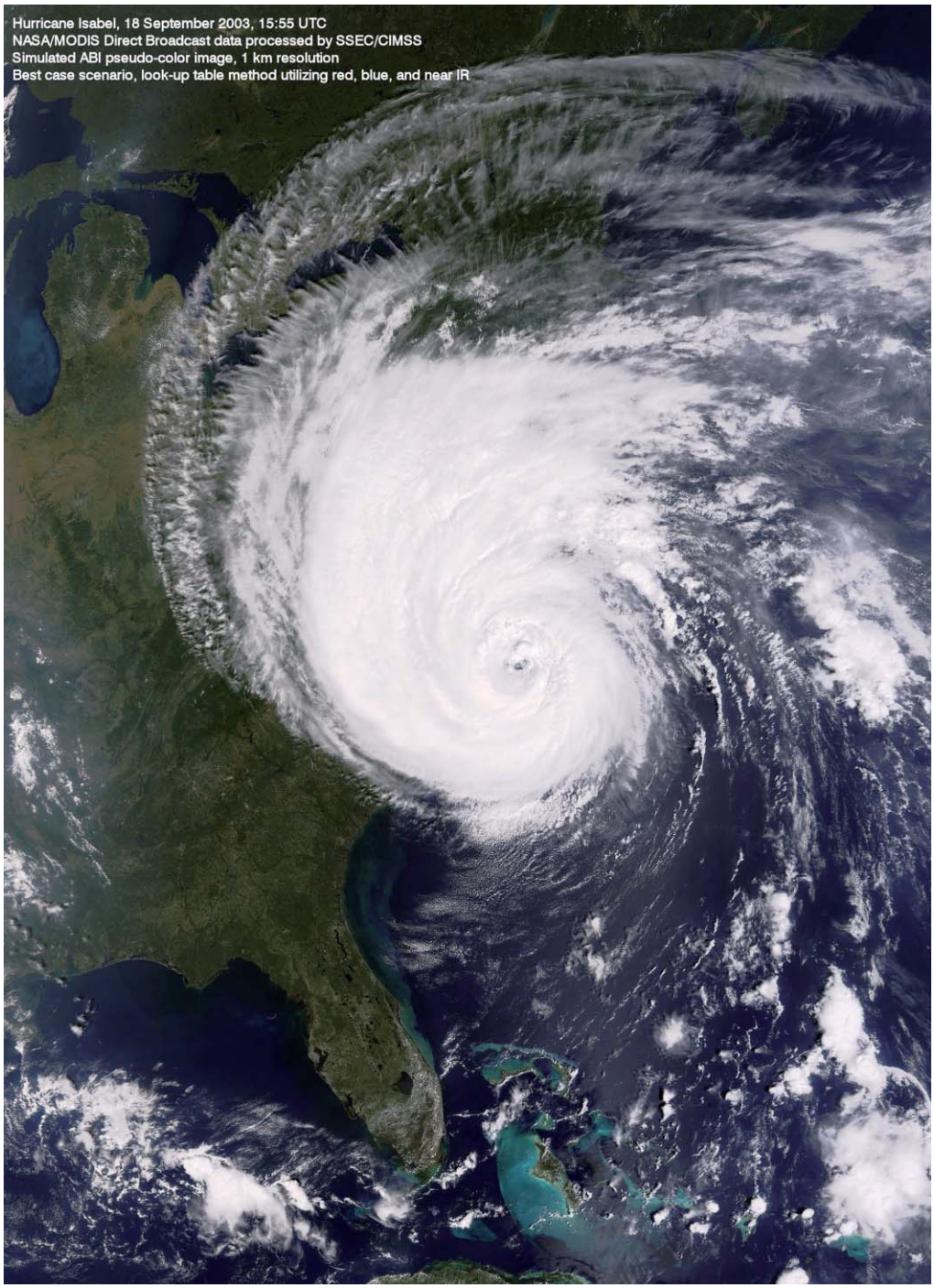


**Fig. 1** Simulated-ABI pseudo-color image featured on the GOES-R.gov website and associated public relation brochures. This is a 1 km resolution image with a static color background obtained from MODIS imagery. (Image courtesy of Chris Schmidt, CIMSS).

true-color imagery anticipated from the ABI is presented, in the context of numerical weather prediction model simulations of ABI for cloudy atmospheres. The process involves two steps: first, the generation of synthetic-green data for ABI; and second, the production of true-color (RGB) imagery by using that synthetic-green band. This work is the first formal application of the green look-up-tables (LUT's) technique to simulated ABI data.

**Fig. 2** GeoColor imagery from the *NexSat* website. The static color background is composed of images from NASA's blue marble (MODIS data) and current GOES visible and infrared data overlaid via dynamic transparency factors.

## 2 Synthetic-Green Image Production

For satellite instruments that do not include a green band, but do possess the other two requisite bands for true-color imagery, the generation of a green image from other spectral bands is a straight-forward process. This can be accomplished by leveraging existing multi-spectral satellite data for which the green image is already available. The MODIS sensors on board NASA's Earth observing system Terra and Aqua satellites, which have red, green, and blue visible bands, can be used for this purpose.

Miller et al.[5] presented such a method for synthesizing a green band (with an eye toward GOES-R true-color applications) from three nearby bands: red, blue, and near-IR (0.86 $\mu$m) bands, similar to those that will be available on the GOES-R ABI. The process for synthesizing the green band involves generation of scene-dependent LUTs based on available imagery from MODIS. The LUTs have three dimensions, with axes in the red, blue, and near-IR directions. The LUT is populated with MODIS-observed green-band reflectances according to the simultaneously-observed red, blue, and near-IR values of reflectance. The LUT considers a broad composite of MODIS imagery from a wide variety of scenes and seasons, including both cloudy and clear-sky scenes.

Once the LUT is developed, it is just a matter of using the ABI red, blue, and near-IR image reflectance values to query the LUT for an equivalent value of green-band reflectance. If the LUT were fully populated, it would always return a green reflectance. However, because of gaps in the LUT due to incomplete population, there are times when a green reflectance needs to be computed from nearby LUT entries. This is done iteratively in the Miller et al.[5] algorithm by searching for green reflectances through the use of a gradually-expanding box of red, blue, and near-IR entries until one or more green reflectance are found. The average of those values is then assigned as the green reflectance.

### *2.1 RGB (True-Color) Imagery*

After the red, green, and blue images are available, the generation of true-color imagery is straightforward. Most image processing systems have built-in ways of combining images with colors applied to the image components. RGB images can be made from any combination of the satellite spectral bands. Most of these combinations result in false-color images, in that the red, green, and blue color planes are applied to spectral bands other than those in the red, green, and blue parts of the visible spectrum respectively. However, by applying the red, green, and blue directly to the red, green, and blue visible bands, and scaling these bands appropriately

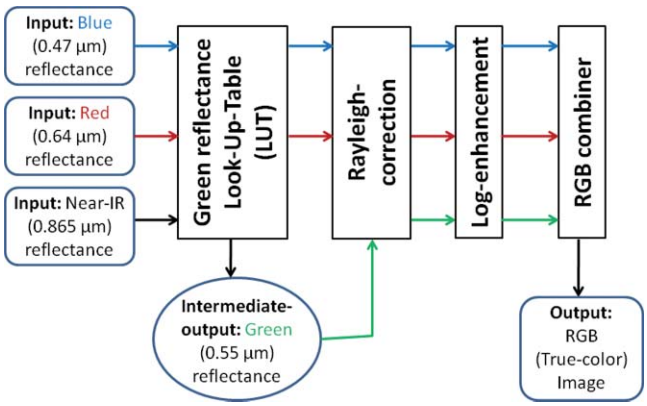


**Fig. 3** High-level flowchart for generating true-color/RGB images, with application of green-LUT, followed by Rayleigh-correction, followed by log-enhancement.

to simulate to first-order the response of the human eye, the result will be a true-color image.*

The order of processes in generating the green band image and resulting RGB image is presented as a flowchart in Fig. 3. After the green LUT is applied, both Rayleigh-correction and log-enhancement steps can be applied to the red, green, and blue bands to brighten the resulting RGB (true-color) image.

As an example the green LUT applied to MODIS data, the top image in Fig. 4 is a synthetic true-color (synthetic-RGB) image generated using the synthetic-green band computed from the MODIS red, near-IR, and blue bands; whereas the bottom image is a true-color (RGB) image generated using the observed-green band from MODIS. These images of the oceans to south and east of Florida, with particularly colorful shoals as observed from space, are a good challenge for testing synthetic-true-color versus true-color based on the current technique. Although the reproduction using synthetic-green is quite good at first glance, there are areas of disagreement when the two images are inspected closely. Note for example, the centers of some of the lagoons where the synthetic-RGB image does not contain the green colors of the observed-RGB image. Miller et al.[5] attempted to improve the performance of the synthetic-green algorithm in these challenging areas (where correlation between green and the available ABI bands are weak, at best) via surface-dependent look-up-tables, but obtain only limited success.

There are two ways to compare the synthetic-RGB and observed-RGB images. One approach is to calculate the differences in green reflectances, as those are the only parts of each image that have changed. That reflectance difference (synthetic-green minus observed-green) is provided as an image in Fig. 5, where positive differences are shaded red and negative differences are shaded blue. The difference scale at the bottom ranges from –0.1 to 0.1 (with typical red and blue differences on the order of 0.05). When compared to observed reflectances in the scene, the differences range from as little as 1% (for clouds, where the absolute reflectances are high) to as much as 10% (for land, where the absolute reflectances are much lower). The difference image exhibits both red areas (positive differences) that are greener and blue areas (negative differences) that are less green. With more blue than red, there appears to be a general bias toward less green in the synthetic-green band. But this difference is subtle and much harder to see in the RGB images that were shown in Fig. 4.

*Note: Man computer interactive data access system (McIDAS) systems have RGB capability, to create 24-bit color images from 8-bit red, green, and blue images. But the McIDAS RGB images are not amenable to further image looping and manipulation within McIDAS. Therefore, software is available[2] that overcomes that limitation, turning RGB images into 8-bit McIDAS-formatted AREA files.

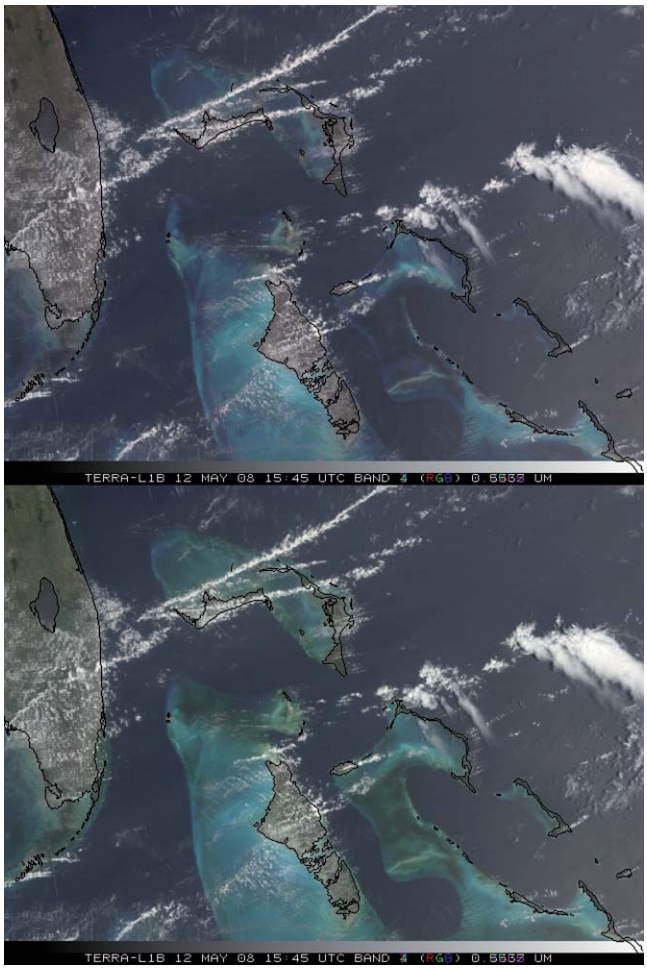


**Fig. 4** MODIS RGB images of the Bahamas: (Top) RGB image generated using a synthetic-green component; (Bottom) RGB image generated with the green-band observed by MODIS. Note a few areas in the top image, in the centers of some of the lagoons, where the green colors are not reproduced correctly, compared to those in the bottom image. A Rayleigh correction has been applied to the images to remove atmospheric absorption and enhance the colors.

Another way to compare the synthetic-RGB and observed-RGB images is through a mathematical transformation of the RGB color space. Hue is one of the three components created during an RGB to hue, saturation, and value (HSV) transformation.[6] The RGB to HSV transformation is briefly described in Appendix A. The hue for a colored pixel is its predominant color in the RGB spectrum, or the main attribute of a color which distinguishes it from other colors.

The images in Fig. 6 depict the hue component when given at full color saturation. The Hue therefore strongly amplifies differences in color. By using hue transformation of the synthetic-RGB and observed-RGB images, differences between the images are amplified. Most areas in the hue images are blue because of the predominance of atmospheric scattering and tendency toward blue light. However, land and ocean colors other than blue still appear. When comparing the two hue images, the shallow lagoon areas that were noted as less green by image differencing (Fig. 5), are also less green in the hue images, more clearly confirming that they are less green in the synthetic-RGB image compared to the observed-RGB image. The hue transformation of RGB images will be used again later to compare and assess RGB images for ABI as generated from model output.

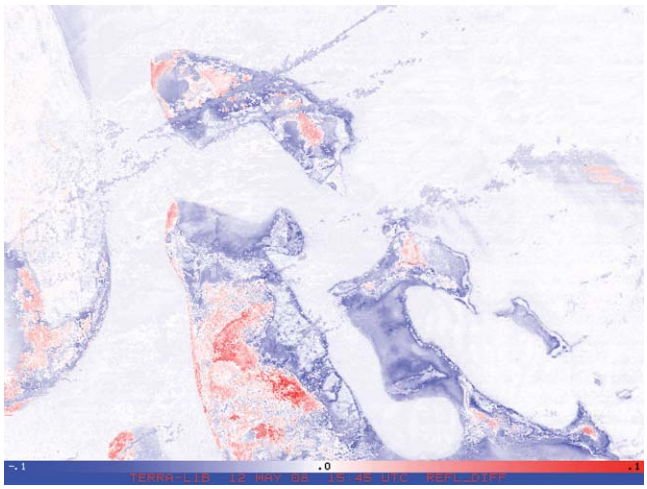

**Fig. 5** Reflectance difference image created by subtracting the "real" green image from the synthetic-green image (from Fig. 4), and scaled from –0.1 (blue) to +0.1 (red). Red areas (positive differences) are greener, whereas blue areas (negative differences) are less green. Areas with little or no difference are white. Note that the larger differences are over the shallow lagoons, where some areas are greener (red) and other areas are less green (blue).

## 3 Production of Simulated ABI

Until GOES-R is launched in 2015 and commissioned to operations, data matching the ABI spectral response functions and spatial (0.5-km visible) and temporal (5 min) resolution are only available through simulations, not from any other satellite. These data, formed by coupling numerical weather prediction model fields with a forward radiative transfer model designed to simulate the ABI measurements, can be used to synthesize the green band, and produce true-color (RGB) imagery. The reason for synthesizing the green band from the simulated ABI bands, rather than simply simulating a green band directly, is to most realistically capture the predicted appearance and behavior of the operational ABI capability. This is done with the realization that any approximation such as synthetic-green will be accompanied by an assortment of caveats, which can be anticipated via the simulated imagery. We therefore follow an approach here that is as close to the operational implementation as possible.

Simulations of ABI imagery can be realized by spectrally transforming images from other satellites, such as MODIS, or by radiative transfer modeling. The spectral-transform method (not the path taken in this work) allows the direct production of both ABI and green-band imagery for use as ground truth. Likewise, the radiative-transfer method offers the ability to simulate both ABI and green-band imagery that can also be used as a form of ground truth. The use of simulated ABI data to test the generation of true-color imagery from ABI is unique to this work, whereas in Miller et al.[5] the technique is applied to MODIS data only.

### *3.1 RAMS Simulations of ABI Visible/Reflective Bands*

In the first case presented, the regional atmospheric modeling system (RAMS)[7] was used to simulate the atmosphere over a section of the north central United States on June 27, 2005. RAMS was initialized and nudged with the North American regional reanalysis dataset.[8] A total of three grids were used, with the innermost nested grid having horizontal grid spacings of 2 km in both horizontal directions. Model output for several ABI infrared spectral bands was generated at 5 min intervals to match the temporal frequency of GOES-R ABI regular northern hemisphere scans. For the illustrative purposes of this study, only the simulated GOES-R ABI

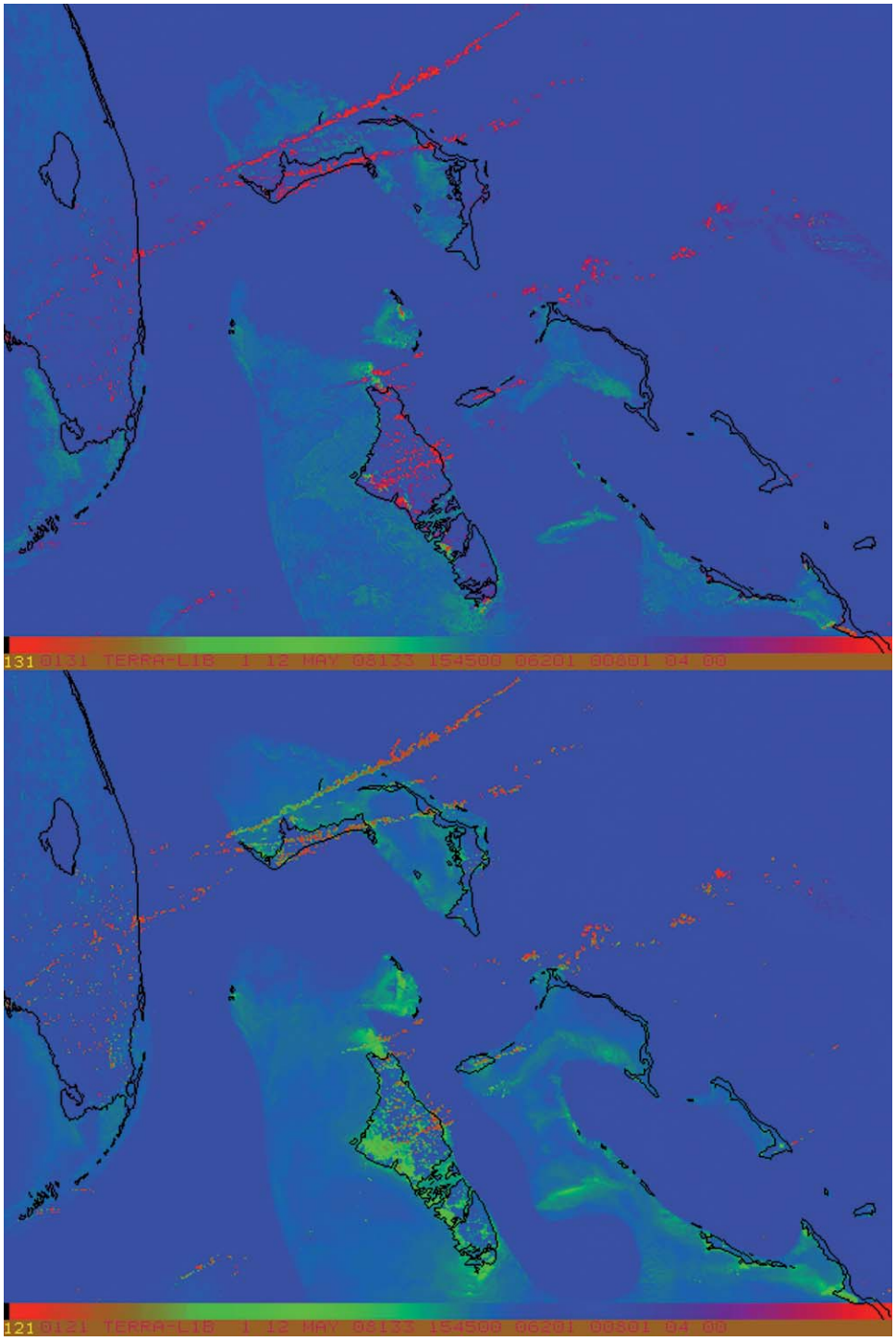

**Fig. 6** Hue images created from the RGB images in Fig. 4. Top hue image was created from the synthetic-RGB image and the bottom hue image was created from the observed-RGB image. These images show the predominant color for each pixel in an image when displayed at full saturation. Note that overall there is less green in the top image created from the (top) synthetic-RGB image in Fig. 4, as well as in some of the shallow lagoons where differences were already noted.

visible band imagery from 2000 UTC images will be shown and discussed, to be later compared and contrasted with available MODIS imagery at 2000 UTC.

The output from RAMS was used as input to a radiative-transfer model,[9] in order to calculate radiances at 0.47 $\mu$m (blue), 0.64 $\mu$m (red), and 0.865 $\mu$m (near-IR). A one-dimensional version of the spherical harmonic discrete ordinate method (called SHDOMPP[10]) was used to compute top of the atmosphere radiances of these three bands. SHDOMPP requires surface albedos as a lower boundary condition. These surface albedos were acquired from the MODIS 16-day albedo product.[11–13] Albedos were mapped from the MODIS grid onto the RAMS grid and subsequently used by SHDOMPP. These data essentially provide the background or "coloration" observed in the simulated imagery to follow.

### 3.2 Results of Simulations

RAMS-simulated ABI visible/reflective images were generated over the north central United States, containing a wide variety of land types, in a scene extending from less-vegetated regions around the Black Hills and just east of the Rocky Mountains, into more-vegetated areas of Wisconsin and Illinois. Clouds were included in the simulations, but few clouds interfered with the land surfaces where color variations will be seen.

The individual red, near-IR, and blue band simulations were performed and the green image was synthesized from those bands using the LUT method described earlier. Rather than showing individual simulated bands in black and white, only the resulting RGB (true-color) image will be shown, since color makes it easier to assess the image quality and is the principal objective of this exercise.

The resulting simulated ABI synthetic-RGB image at 2000 UTC on June 27, 2005 is shown as the top image in Fig. 7, along with enhanced versions of the same image below. The enhancements not only brighten the original image, but also make it easier to see more subtle variations in the colors of the land features. The enhancement applied to the RGB image is an atmospheric/Rayleigh-correction.[14] The Rayleigh-correction is typical of enhancements applied to MODIS true-color imagery. After the Rayleigh-correction is applied, a log-enhancement is applied as well, as an important step in true-color image processing because it approximates human vision response.

Only the synthetic-RGB versions are shown in Fig. 7, since the directly-simulated RGB images are hard to distinguish from the synthetic-RGB images, even when placed side-by-side.

For easier comparison of synthetic-green with simulated-green, Fig. 8 displays the hue images for the synthetic-RGB and simulated-RGB images, on top and bottom, respectively. By contrasting these hue images, it can be seen that the synthetic-RGB image (on the top) contains less green than the directly-simulated RGB image (on the bottom), at least over vegetated surfaces. The less-green aspect to the synthetic-RGB is in agreement with the green look-up-tables (LUTs) application to MODIS already presented. In contrast to the green hues, less vegetated surfaces in central Wyoming, eastern Colorado, and western Nebraska and some of the higher cloud tops on the right side of the images have red hues. The red hue of the higher clouds in particular was also seen in the MODIS hue images.

HSV analysis clearly confirms the less-green bias, by giving a sense of the true/basic color of land features in particular. Small or subtle differences in RGB imagery appear as large differences in hue, due to the transformation from RGB color space to HSV color space. Hue analysis can quickly reveal issues in the generation of green and RGB images, especially in the comparison of RGB images created from both observed-green and synthetic-green images.

For comparison with the simulated ABI data, real MODIS data for the same day and time (2000 UTC) is shown in Fig. 9. The MODIS data has been remapped into the ABI projection, and the image is presented in only one version, the Rayleigh-corrected and log-enhanced enhanced

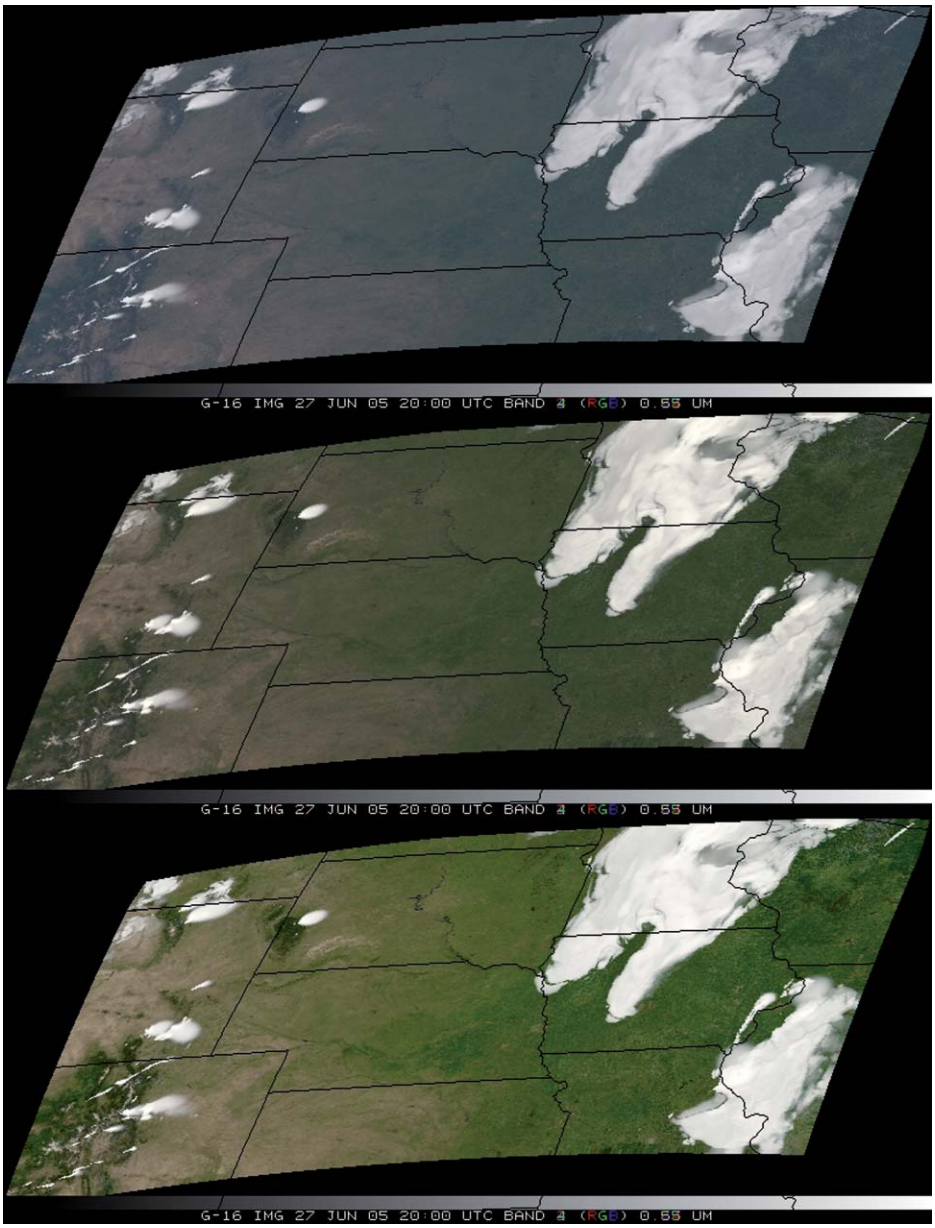


**Fig. 7** Example of simulated ABI synthetic-RGB images for June 27, 2005 at 2000 UTC: (top) no enhancement; (middle) Rayleigh-correction applied; (bottom) Rayleigh-correction and log-enhancement applied. Only the RGB images with the synthetic-green component are shown here, as it is hard to distinguish these from the RGB images with the directly-simulated green component.

image, to be compared to the bottom ABI image in Fig. 7. The MODIS image contains real clouds, compared to the model-generated clouds in the ABI simulations. However, clouds are not the main focus of these ABI simulations. Rather, the colored land surfaces are of interest, and those surfaces, particularly on the left side of the image, appear to have similar colors between simulated-ABI and MODIS. However, on the right side of the MODIS image, with data from near the edge of the MODIS granule, the satellite viewing angles are very large, resulting in much scattering and a blue/green tint to the image, unlike the simulated GOES-R ABI image

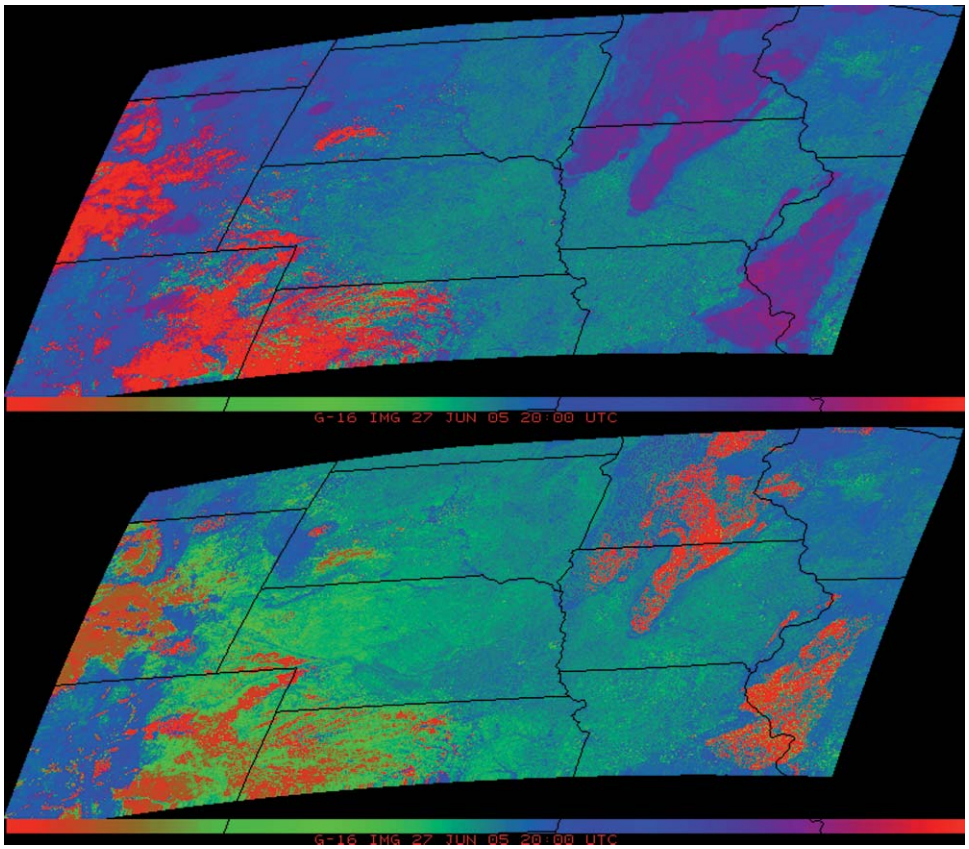


**Fig. 8** Hue images for the synthetic-RGB and simulated-RGB images for the same time as in Fig. 7. Both hue images are for non-Rayleigh-corrected RGB images. These hue images emphasize the difference between the synthetic-RGB and simulated-RGB images, as seen by the less-green hue of most vegetated surfaces in the synthetic-RGB (top) image. Less vegetated land surfaces are red in both images (along with the larger cloud tops).

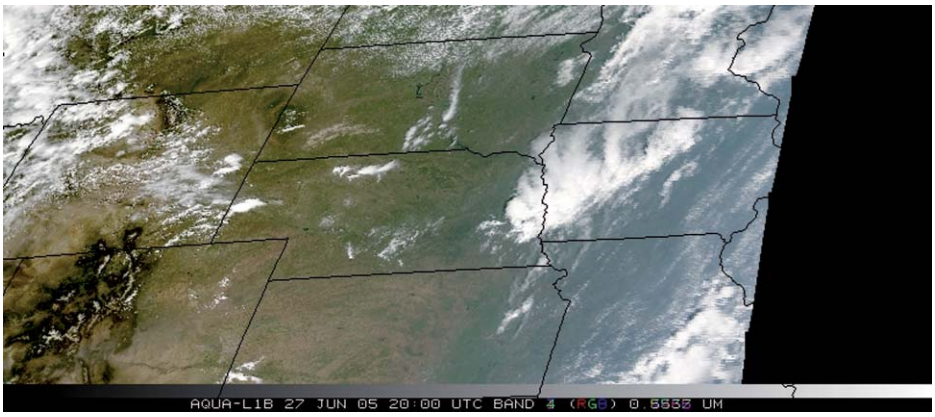


**Fig. 9** MODIS RGB image mapped to the ABI projection and for the same time (2000 UTC) as the ABI images in Fig. 7. These MODIS images contain real clouds as opposed to the model-generated clouds in the ABI simulations. Only the Rayleigh-corrected and log-enhanced version of the image is shown.

in Fig. 7, where satellite viewing angles are much more vertical, and the whole image contains similar land-surface colors.

### 3.3 Quantitative Reflectance Comparisons

Up to this point, image differencing and variations in hue images have been used to compare the synthetic-RGB images from RAMS to directly-simulated RGB images created from direct-simulations of the ABI green band. These direct-simulations of the green band were made for the purpose of providing a form of "ground truth" for the synthetic-green band produced by the LUT methodology. When the two versions of the Green band are combined into their respective RGB images, a slightly-less-green bias was observed in the synthetic-images (based on this implementation of the Miller et al.[5] technique) compared to the directly-simulated images.

For a quantitative comparison of the simulated component images, statistics were computed on the simulated ABI reflectances, as well as on the observed MODIS reflectances for the same day and time in the example already presented. The results are given in Table 1. Rows in the table are for the blue, red, near-IR, (observed) green, and synthetic-green bands. Columns 3 and 5 give the MODIS and ABI band numbers for each color. The MODIS 16-day albedos (column 4) are the lower boundary conditions applied over the entire scene, used to compute the model-simulated ABI reflectances (column 6). Finally, the observed MODIS reflectances for this case are available in column 7. All the reflectances are given in percent form, rather than as reflectances from 0 to 1.

To compute the statistics in Table 1, a cloud-free area in both the ABI and MODIS images covering 10000 pixels, over most of central Kansas, was chosen. This cloud-free sub-area does not necessarily have the full variability of the entire scene, as is clear from the lower standard deviations for the simulated ABI reflectances compared to the underlying MODIS 16-day albedos for the entire scene. However, computing the statistics on only this smaller sub-area is necessary to avoid cloud-contaminated values.

In Table 1, a comparison can be made between the simulated ABI reflectances and the observed MODIS reflectances, as found in the last two columns. The averages of the ABI reflectances are similar to, but in general less than, the averages of the MODIS reflectances, in most bands (blue, red, and green), except for the near-IR band, where the ABI reflectances are greater than the MODIS reflectances. Among all the bands, the greatest relative difference between ABI and MODIS is associated with the Blue band, where the average ABI reflectance is 11.8% and the average MODIS reflectance is 13.5%. This larger difference for blue is likely associated with increased atmospheric scattering at these shorter wavelengths, compared to much less scattering at longer wavelengths for all the other bands.

Table 1 also compares the ABI reflectances in the directly-simulated green image with those in the synthetic-green image, as the last two rows in column 6. The lower reflectances in the synthetic-green band, 11.7% versus 12.4%, or 0.7% less, agrees with the less-green bias found

**Table 1** Reflectance statistics for simulated ABI versus MODIS.

| Color | Wavelength $\mu$m | MODIS band | MODIS 16-day albedo average (std dev)% | ABI band | Simulated ABI reflectance[a] average (std dev) % | MODIS reflectance[a] average (std dev) % |
|---|---|---|---|---|---|---|
| Blue | 0.47 | 3 | 4.1 (2.1) | 1 | 11.8 (1.0) | 13.5 (0.8) |
| Red | 0.64 | 1 | 7.6 (3.8) | 2 | 11.3 (2.2) | 12.3 (2.1) |
| Near-IR | 0.86 | 2 | 37.3 (7.3) | 3 | 31.5 (3.0) | 29.7 (2.8) |
| Green | 0.55 | 4 | 8.8 (2.5) | – | 12.4 (1.1) | 12.8 (0.9) |
| Synthetic-green | 0.55 | – | Same as above | – | 11.7 (1.1) | 12.9 (0.9) |

[a]Statistics computed on a 10000 pixel sample of cloud-free simulated ABI and MODIS covering central Kansas; whereas the MODIS 16-day albedos statistics apply to the entire scene.

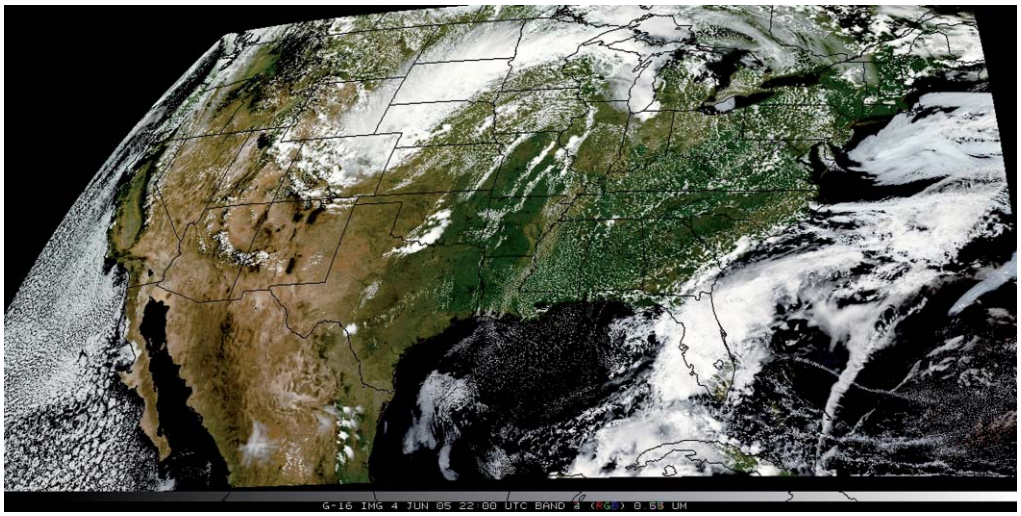


**Fig. 10** Synthetic-RGB imagery from WRF-simulations of ABI over the continental United States. The ABI visible/reflective band imagery for this case was provided by CIMSS, from which the green band (not shown) and RGB image were generated. Both a Rayleigh correction and a log enhancement have been applied to enhance the image.

using the other methods already applied to assess the synthetic-RGB images created for ABI. However, the statistics for simulated ABI and observed MODIS are not expected to be identical due to simulation and spectral response differences. Finally, a comparison between the green and the synthetic-green generated for MODIS, with values of 12.8% and 12.9%, respectively, does not show the less-green bias for this case.

### *3.4 Additional Example of WRF-Generated ABI*

As an alternative to the RAMS model simulations, simulated ABI reflective band imagery was obtained from the Cooperative Institute for Meteorological Satellite Studies (CIMSS) at the University of Wisconsin–Madison, for use in testing of both the synthetic-green band and synthetic-RGB imagery. The CIMSS simulations used the weather research and forecasting (WRF) model to create imagery over the continental United States.[15] The resulting synthetic-RGB image is shown in Fig. 10, a larger continental U.S. example of true-color capability for future ABI. The larger scale and lower resolution of this example creates an eye-appealing image. The image was likewise enhanced using both the Rayleigh correction and log enhancement that was used for earlier RGB images. For this case, the green band was not directly simulated, so it was only available synthesized from the other ABI reflective bands. Therefore, no comparisons between synthetic-green and directly-simulated green were possible.

### *3.5 Adding Smoke to Simulated ABI*

One application of true-color imagery is the detection of aerosols, in particular smoke from wild fires. As an extension to the model simulations of RGB images for ABI, work is just beginning on adding smoke and other extinction media to the simulated ABI data. An example of a smoke plume added to the ABI simulations of fires over southern California is shown in Fig. 11. The shape of the "plume" was taken from MODIS imagery for this day, during which northeasterly winds were blowing the smoke offshore.

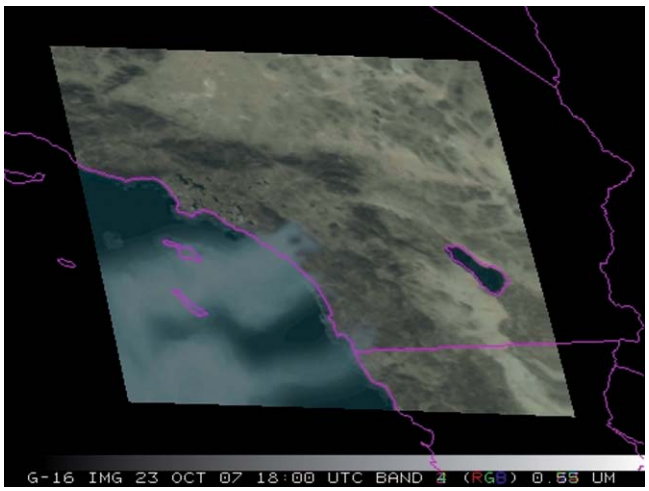


**Fig. 11** Simulated ABI image with added smoke for October 23, 2007 over Southern California. The smoke plume was added to the individual component images, resulting in this RGB image. A Rayleigh correction has been applied to enhance the image.

Adding a plume to the imagery required specifying the spectrally dependent optical properties for smoke. In this case, optical properties were acquired from Reid et al.[16] Extinction values for the four spectral bands, 0.47, 0.555, 0.64, and 0.865 $\mu$m, were $2.26347\times10^{-3}$, $1.62324\times10^{-3}$, $1.2207\times10^{-3}$, and $6.60589\times10^{-4}$ $m^{-1}$, respectively. The single-scatter albedo and asymmetry factor for all bands were held fixed at 0.87 and 0.63, respectively. A scaling factor was derived from a MODIS gray-scaled image of smoke, and that factor was allowed to vary from 0.0 (no smoke) to 1.0 (full smoke). These spectrally independent values were multiplied by the extinction at each wavelength. This gave the smoke plume an optical depth that varied horizontally. Vertically, the smoke plume had constant optical properties at each level where present in the column. For this simulation, a 2 km thick smoke plume was placed into the simulated domain between 1 and 3 km in the vertical.

Similar to the RAMS example already presented, SHDOMPP was used to compute radiance values at each of the four spectral bands (red, near-IR, blue, and green). Surface albedos were derived from MODIS 16-day albedos. Although albedos are not available over the ocean, they are available over the Salton Sea in southern California, and were used as the ocean values for each band. A time of 1800 UTC was chosen for the radiance calculations. This value was chosen to reduce the solar zenith angle in the simulation. As a result, the path length is near a minimum thus reducing the number of calculations and the time required for the simulation of each band.

The synthetic-RGB image distinctly shows the smoke patch over both land and ocean backgrounds. In regions of maximum smoke extinction, the visible reflectances are greatly increased over the reflectances at locations with no smoke. Table 2 gives some details on the

**Table 2** Reflectance statistics for simulated ABI versus MODIS (smoke pixels only).

| Color | Wavelength $\mu$m | ABI band | Simulated ABI reflectance maximum % | MODIS band | MODIS reflectance maximum % |
|---|---|---|---|---|---|
| Blue | 0.47 | 1 | 16.9 | 3 | 19.3 |
| Red | 0.64 | 2 | 12.4 | 1 | 17.2 |
| Near-IR | 0.86 | 3 | 8.1 | 2 | 15.5 |
| Green | 0.55 | – | 14.2 | 4 | 18.1 |
| Synthetic-green | 0.55 | – | 13.8 | – | – |

effect of smoke in the various spectral bands. When compared to MODIS reflectances (last column), the maximum ABI reflectances (column 4) are all lower, but the reflectances decrease in the same color order for both MODIS and ABI, with the largest reflectances in the blue band and the smallest reflectances in the near-IR bands.

The addition of smoke is presented merely as an example of how RGB imagery can be applied to the detection of aerosols. Additional simulations of smoke and other types of aerosols are planned, along with the ability to use RGB imagery for quantifying the detectability of such aerosols. The model simulations allow the entry of both aerosol density and thickness, to test the detection limits for aerosols using the RGB capabilities of future ABI. Current plans are to provide proxy datasets with added aerosols that can be used to test aerosol detection algorithms developed by the GOES-R algorithm working group.[17]

## 4 Summary and Conclusions

True-color RGB satellite imagery has a certain qualitative appeal, not only to the layman, but also to professional forecasters. The spectral components in true-color imagery can facilitate the detection of spectrally-dependent features in both land and ocean surfaces and in the atmosphere. This is why true-color imagery is often featured on NOAA and NASA websites, even though it is currently available only from certain polar-orbiting satellites, and not from current operational geostationary satellites. Nor will true color be a direct product from the future GOES-R ABI either, since the ABI will not provide a green band.

To satisfy the desire for true-color imagery at geostationary temporal refresh rates, methods for the production of true-color imagery from ABI have been developed, including a synthetic-green imagery approach that is evaluated here. The missing green information is synthesized from nearby reflective bands that offer a correlative relationship. Examples were presented of simulated ABI imagery, generated by forward radiative transfer model calculations from two different models: RAMS and WRF.

While the bias is subtle and difficult to assess within the true color imagery itself, image differencing revealed that a less-green bias in synthetic-green reflectance exists in the current LUT method that was utilized for the cases examined, as verified by the statistics performed on the images. Similarly, a color-space transformation from RGB to HSV reveals the less-green bias much more clearly.

Besides the observed bias, other area-dependent discrepancies that were seen in the synthetic-green images are likely caused by deficiencies or nonuniqueness in the green-band LUT. Further improvements to the synthetic-green process might be possible by expanding the training data base of MODIS imagery that went into the LUT that is currently available, or further refining the technique itself via selective (function of region/season/etc.) bias corrections. The low bias might also be alleviated through the use of direct model simulations of the ABI green band to generate an alternative to the MODIS-derived LUT, allowing green band synthesis that is trained on expected ABI spectral characteristics, not MODIS training.

Finally, this limited attempt at adding a smoke plume to simulated ABI indicates that true-color imagery holds a possible advantage for use in determining the limits of detectability for airborne smoke and other aerosols. Forthcoming simulations will provide baseline information on the minimum particle densities and thicknesses that should be detectable from ABI true-color imagery, with a planned application as proxy datasets that can be used to test ABI aerosol detection algorithms.

## Acknowledgements

This research was primarily funded by NOAA's National Environmental Satellite, Data, and Information Service (NESDIS) GOES-R Program Office. We thank C. Schaaf of the MODIS Land Team, for the 16-day albedos that were used as the RAMS model lower boundary. The views, opinions, and findings contained in this article are those of the authors and should not

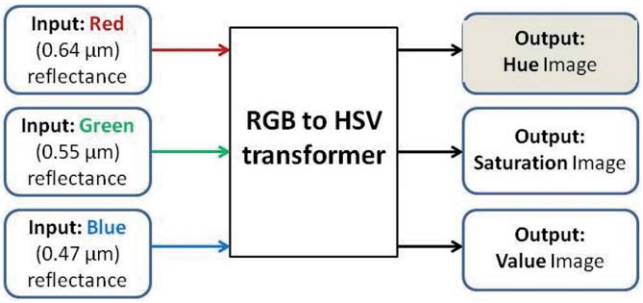


**Fig. 12** High-level flowchart for generating hue, saturation, and value images from RGB component images. Only the hue image is of interest.

be construed as an official National Oceanic and Atmospheric Administration (NOAA) or U.S. Government position, policy, or decision.

## Appendix A: HSV transformation of RGB imagery

There are several cylindrical-coordinate representations of the RGB color model. Those representations mathematically rearrange the geometry of the RGB cube to be more perceptually relevant. The two most common transformations of RGB space are: HSV; and hue, saturation, and lightness (HSL). Although the definition of saturation is different between HSV and HSL, the definition of hue is similar. Hue is the angle around the central axis of the cylinder, whereas

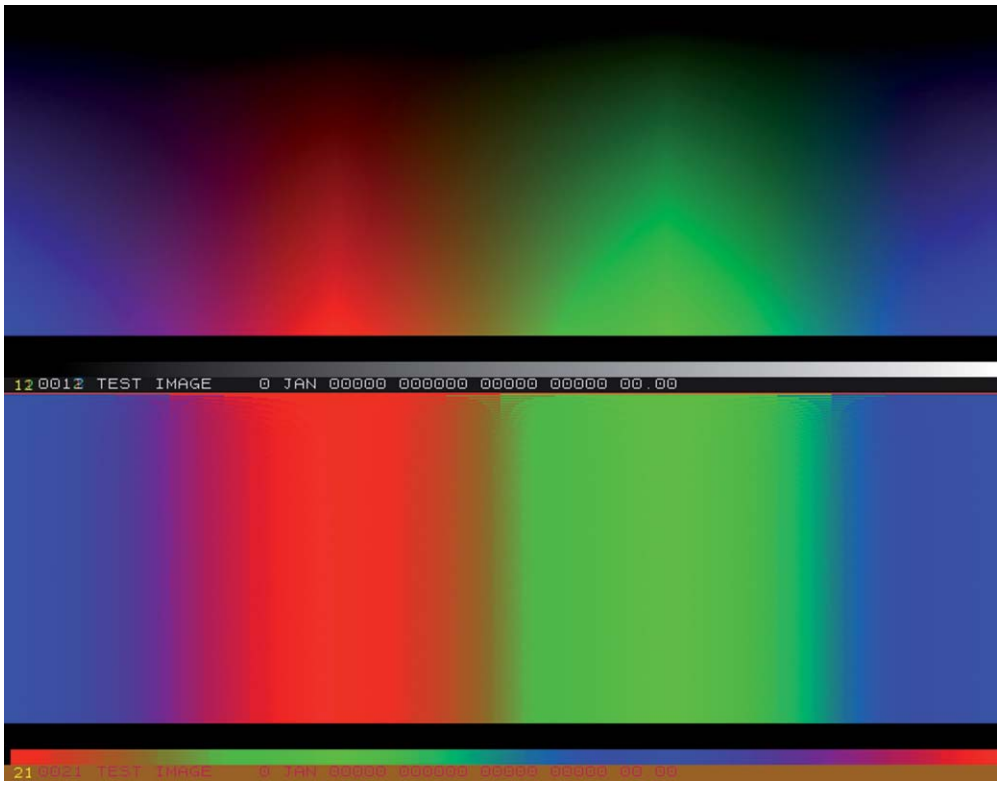


**Fig. 13** (top) RGB test image with red, green, and blue sections, fading from light at the bottom to dark at the top; (bottom) hue image from RGB test image, displaying the same hue regardless of the color saturation or lightness (not shown, but implied by the RGB image).

the saturation (of a color) corresponds to the distance away from that axis of the cylinder, and value (or lightness) of a color corresponds to the distance along the central cylinder axis. Hue can be thought of as the real color, saturation the depth of the color, and value or lightness as the darkness or lightness of the color.

The process for generating HSV imagery from RGB imagery is outlined in the flowchart in Fig. 12.

A graphical visualization of the transformation of RGB imagery into HSV imagery is provided by Jang and Ra.[18] Hue is represented by the rotation angle around the HSV cylinder and is often given an angle for its value. In contrast, saturation and value are generally given values between 0 and 1. Figure 13 is presented to show that the hue is independent of the color saturation. The three red, green, and blue colored sections in the RGB image in the top half are faded vertically from full saturation at the bottom of the image to dark at the top of the image. In the transformation to the hue image in the bottom half, the hues are vertically independent of the saturation level seen in the RGB image in the top half.

The color bar at the bottom of Fig. 12 displays a rotation around the entire 360 deg color wheel, starting and ending with red. Changes in angle of 120 deg result in primary color changes, and even subtle changes between primary colors may be quite noticeable to the eye when viewed in hue space.

A complete understanding of the RGB to HSV transformation is not necessary for this application, since only the hue component is of interest. Hue represents the main attribute of a color which distinguishes it from other colors. When the hue is displayed at full saturation, it can amplify subtle differences both within an RGB image and between RGB images, such as when applied to the RGB images created from simulated GOES-R ABI.

## References


1. S. D. Miller, J. D. Hawkins, J. Kent, F. J. Turk, T. F. Lee, A. P. Kuciauskas, K. Richardson, R. Wade, and C. Hoffman, "*NexSat* – Previewing NPOESS/VIIRS imagery capabilities," *Bull. Amer. Meteor. Soc.* **87**, 433–446 (2006).
2. D. W. Hillger, "GOES-R advanced baseline imager color product development," *J. Atmos. Ocean. Technol. – Atmospheres* **25**, 853–872 (2008).
3. C. Schmidt, personal communication (2009).
4. T. J. Schmit, M. M. Gunshor, W. P. Menzel, J. J. Gurka, J. Li, and A. S. Bachmeier, "Introducing the next-generation advanced baseline imager on GOESR," *Bull. Amer. Meteor. Soc.* **86**, 1079–1096 (2005).
5. S. D. Miller, C. Schmidt, T. Schmit, and D. Hillger, "A case for natural colour imagery from geostationary satellites, and an approximation for the GOES-R ABI," Accepted by the *Int. J. Remote Sens.* (2011).
6. J. G. Liu and J. McM. Moore, "Hue image RGB colour composition. A simple technique to suppress shadow and enhance spectral signature," *Int. J. Remote Sens.* **11**(8), 1521–1530 (1990).
7. W. R. Cotton, R. A. Pielke, Sr., R. L. Walko, G. E. Liston, C. J. Tremback, H. Jiang, R. L. McAnelly, J. Y. Harrington, M. E. Nicholls, G. G. Carrio, and J. P. McFadden, "RAMS 2001: Current status and future direction," *Meteor. Atmos. Phys.* **82**, 5–29 (2003).
8. F. Mesinger, G. DiMego, E. Kalnay, K. Mitchell, P. C. Shafran, W. Ebisuzaki, D. Jovic, J. Woolen, E. Rogers, E. H. Berbery, M. B. Ek, Y. Fan, R. GruhPaine, W. Higgins, H. Li, Y. Lin, G. Manikin, D. Parrish, and W. Shi, "North American regional reanalysis," *Bull. Amer. Meteor. Soc*. **87**, 343–360 (2006).
9. L. D. Grasso, M. Sengupta, J. Dostalek, R. Brummer, and M. DeMaria, "Synthetic satellite imagery for current and future environmental satellites," *Int. J. Remote Sens.* **29**, 4373–4384 (2008).
10. K. F. Evans, "The spherical harmonics discrete ordinate method for three-dimensional atmospheric radiation transfer," *J. Atmos. Sci.* **55**, 429–446 (1998).

11. W. Lucht, C. B. Schaaf, and A. H. Strahler, "An algorithm for the retrieval of albedo from space using semiempirical BRDF models," *IEEE Trans. Geosci. Remote Sens.* **38**, 977–998 (2000).
12. C. B. Schaaf, F. Gao, A. H. Strahler, W. Lucht, X. Li, T. Tsang, N. C. Strugnell, X. Zhang, Y. Jin, J.-P. Muller, P. Lewis, M. Barnsley, P. Hobson, M. Disney, G. Roberts, M. Dunderdale, C. Doll, R. d'Entremont, B. Hu, S. Liang, J. L. Privette, and D. P. Roy, "First operational BRDF, albedo and Nadir reflectance products from MODIS," *Remote Sens. Environ.* **83**, 135–148 (2002).
13. C. Schaaf, J. V. Martonchik, B. Pinty, Y. Govaerts, F. Gao, A. Lattanzio, J. Liu, A. H. Strahler, and M. Taberner, "Retrieval of surface albedo from satellite sensors," in *Advances in Land Remote Sensing: System, Modeling, Inversion and Application*, S. Liang, Ed., Springer, Dordrecht, The Netherlands, 219–243 (2008).
14. Z. Ahmad and R. S. Fraser, "An iterative radiative transfer coded for ocean-atmosphere systems," *J. Atmos. Sci.* **39**, 656–665 (1982).
15. J. A. Otkin, T. J. Greenwald, J. Sieglaff, and H.-L. Huang, "Validation of a large-scale high-resolution WRF model simulation using SEVIRI satellite observations," *J. Appl. Meteor. Climatol.* **48**, 1613–1626 (2009).
16. J. S. Reid, T. F. Eck, S. A. Christopher, R. Koppmann, O. Dubovik, D. P. Eleuterio, B. N. Holben, E. A. Reid, and J. Zhang, "A review of biomass burning emissions part III: intensive optical properties of biomass burning particles," *Atmos. Chem. Phys.* **5**, 827–849 (2005).
17. X. Zhang, S. Kondragunta, C. Schmidt, and F. Kogan, "Near real time monitoring of biomass burning particulate emissions (PM2.5) across contiguous United States using multiple satellite instruments," *Atmos. Environ.* **42**, 6959–6971 (2008).
18. J. H. Jang and J. B. Ra, "Pseudo-color image fusion on intensity-hue-saturation color space," *IEEE International Conference on Multisensor Fusion and Integration of Intelligent Systems*, Seoul, Korea, pp. 366–371, August 20–22 (2008).

**Donald W. Hillger** earned a BS in physics (1973) from the University of Minnesota, and MS (1976) and PhD (1983) in atmospheric science from Colorado State University. He continued as a post doctoral fellow and later as a research associate at the Cooperative Institute for Research in the Atmosphere (CIRA) at Colorado State University before joining the regional and mesoscale meteorology (RAMM) branch of NOAA/NESDIS as a research meteorologist in 1987. He specializes in satellite meteorology from geostationary and polar-orbiting platforms, as well as satellite instrument calibration/validation, satellite data/image quality, and planning for advanced and future instrumentation. He has published many scientific journal publications, technical reports, and has made presentations at numerous national and international scientific meetings. Publications include journal articles, conference papers and presentations, technical reports, and in-house publications. Current research emphasis includes analysis of multispectral and hyperspectral imagery and the development of image products from those datasets, utilizing computer-intensive analysis methodology. Other emphasis includes the science checkout of operational geostationary satellites (such as GOES) after launch.

**Louie Grasso** received his BS in meteorology from Lyndon State College in 1985. Both his MS (1993) and PhD (1996) in atmospheric science were obtained from Colorado State University. His areas of interest include numerical modeling, satellite meteorology, and severe thunderstorms. Since 1997 he has worked at CIRA where his initial focus was on the numerical modeling of severe storms and soil moisture impacts on dryline development. His dryline work led to a contribution in the Encyclopedia of Atmospheric Sciences. His interests moved into the area of producing synthetic satellite imagery from numerical model output. For the past few years, he has focused primarily on generating synthetic NPOESS VIIRS and GOES-R ABI imagery for a variety of weather and environmental events: Severe storms, lake effect snow, hurricanes, and wild fires.

**Steven Miller** received his BS in electrical and computer engineering from U.C. San Diego (1995), and MS (1997) and PhD (2000) in atmospheric science from Colorado State University. His areas of interest include satellite-based remote sensing of the Earth/atmosphere system from a wide assortment of sensor technologies including active/passive systems spanning the optical to microwave portions of the electromagnetic spectrum. From 2000 to 2007, he worked at the Naval Research Laboratory in Monterey, California in the Satellite Meteorological Applications Section, where he developed numerous value-added satellite imagery tools for operational users (including mineral dust, snow cover, cloud optical properties, low cloud/fog, fire, thin cirrus, deep convection, natural color, contrail, volcanic ash, and nighttime low-light applications). His mineral dust detection algorithms for MODIS and SeaWiFS were among the first to exploit blue-band absorption properties. In 2005, he published the first satellite detection of a widespread bioluminescence phenomenon (the "Milky Sea") using the DSMP Operational Linescan System. He joined CIRA in 2007 as a research scientist and deputy director, where he continues work in developing satellite techniques geared toward operational end-users.

**Renate Brummer** received the equivalent of a MS in mathematics and physics from the Universität München, Munich, Germany in 1981 and a PhD in meteorology and physical oceanography from the University of Miami, Florida in 1986. Her areas of interest include mesoscale forecast modeling, satellite meteorology, and environmental education/outreach. She has been a CIRA employee since 1995 and has been working as project manager for different CIRA projects. During those years she managed the systems development team for the international school program GLOBE. The GLOBE Program is a worldwide community of students, teachers, scientists, and citizens working together to better understand, sustain, and improve Earth's environment at local, regional, and global scales. She also managed the so-called FX-Net project, a meteorological forecaster workstation which provides the user interface and functionality of the AWIPS workstation (used by NWS forecasters) via the internet. During the last two years, she worked as a project coordinator for CIRA's regional and mesoscale meteorology branch (RAMMB).

**Robert DeMaria** received his BS in computer science from Colorado State University (2006). While a CSU student he worked as a student hourly at CIRA. During this time he was responsible for performing data processing jobs and miscellaneous programming support tasks. During the fall of 2006, he was the teaching assistant for the senior level computer graphics course at CSU. In 2007 he joined CIRA as a research associate I.